Analyst

PAPER

View Article Online
View Journal

Cite this: DOI: 10.1039/c7an00586e

K-junction structure mediated exponential signal amplification strategy for microRNA detection in electrochemiluminescence biosensor

Xue Li, Anyi Chen, Yaqin Chai* and Ruo Yuan *

Based on the novel designed K-junction structure, an economic and efficient exponential signal amplification strategy with simple protocol combining hemin/G-quadruplex, a mimetic peroxidase, as a catalyzer was proposed and utilized in an electrochemiluminescence biosensor for sensitive microRNA detection. It was noteworthy that the K-junction structure was formed with guanine-rich reporter DNA and substrate DNA modified by phosphate at the 5′-terminus. Thus, the activity of the reporter DNA could be inhibited and the recognition domain for the target microRNA constructed through the K-junction structure formed. When the target microRNA was sensed, the paired domains of the substrate DNA was completely digested from the 5′-terminus, accompanied by the release of the target microRNA and unpaired DNA fragment of the substrate DNA called the trigger DNA. Afterwards, the released microRNA and trigger DNA were recycled over and over causing the linear and exponential digestion of the K-junction structure, respectively. As a result, numerous uninhibited reporter DNAs were left on the electrode to capture hemin with the yielded hemin/G-quadruplex, which could enhance the ECL emission significantly due to its catalysis for the luminol–H_2O_2. As expected, this method exhibited excellent specificity and high sensitivity for microRNA detection from 0.033 fM. What's more, the application in human lung cancer cell lines achieved good sensitivity for 10 tumor cells.

Received 8th April 2017,
Accepted 2nd May 2017

DOI: 10.1039/c7an00586e

rsc.li/analyst

Introduction

MicroRNAs (miRNAs) have turned out to be important regulators of various biological processes and biomarkers for early disease diagnosis.[1,2] Considering the intrinsic characteristics of miRNAs, such as highly homologous sequences and low abundance in cells, it is full of challenges to achieve sensitive and selective miRNAs detection.[3,4] Up to now, to improve the sensitivity and selectivity, numerous signal amplification strategies have been developed in nucleic acids analysis and protein detection, such as hybridization chain reaction (HCR),[5,6] rolling circle amplification (RCA)[7,8] and strand displacement amplification (SDA).[9,10] Among these previous amplification strategies, exponential amplification strategies have attracted the attention of investigators for their higher amplification efficiency than linear signal amplification strategies. Zhang and co-workers put forward an exponential SDA strategy in an aptasensor using the product DNA of a linear SDA as the primer of another linear SDA.[11] However, this exponential SDA was mediated by two enzymes, which complicated the protocol. Li's group reported an exonuclease-assisted cascade liberating reporter by digesting hairpin inhibitor DNA to realize an exponential signal amplification for DNA detection.[12] However, due to the specific stability of the hairpin motif, this strategy was just suitable for nucleic acid molecule detection with relative few bases. Therefore, it is of great significance to develop a high efficiency exponential signal amplification strategy for sensitive target sensing.

Electrochemiluminescence (ECL) assays have been extensively applied in many areas, such as nucleic acids detection and immunodetection because of their simplified operation, wide detection range, controllable reaction system, short time consumption and high sensitivity.[13–17] Currently, the luminol/H_2O_2 ECL system is one of the most popular ECL systems in practical analyses because of its high light emitting quantum yield, low oxidation, moderate price and non-toxicity.[18] To enhance the ECL emission of the luminol/H_2O_2 ECL system, electrochemical catalysis strategies have played an important role to produce a high enhancement efficiency. However, traditional nano-catalysts, such as cobalt nanoparticles, platinum nanoparticles, magnetic nanoparticles and cerium oxide nanoparticles, suffers the problems of low kinetic efficiency and inconvenient labeling, which limit their performance and applications.[19–22] Hemin/G-quadruplex, formed by the complexation of hemin with a guanine-rich single-stranded nucleic

Key Laboratory of Luminescent and Real-Time Analytical Chemistry (Southwest University), Ministry of Education, College of Chemistry and Chemical Engineering, Southwest University, Chongqing 400715, China. E-mail: yqchai@swu.edu.cn, yuanruo@swu.edu.cn; Fax: +86-23-68253172; Tel: +86-23-68252277

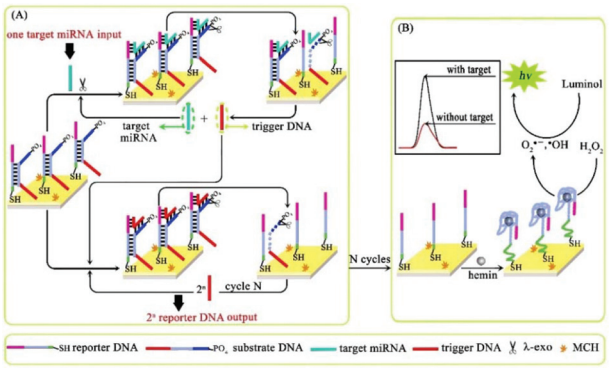

Scheme 1 A schematic representation of the biosensor used for miRNA detection: (A) target miRNA induced exponential signal amplification; (B) the ECL measurement used for the detection of miRNA and the catalysis mechanism of the hemin/G-quadruplex in the luminol/H_2O_2 ECL system.

acid, is a functional DNA structure, which exhibits specific mimicking peroxidase activity to catalyze the decomposition of H_2O_2 much more efficiently.[23] Recently, our group used a hemin/G-quadruplex to achieve excellent performance in the ECL enhancement of the luminol/H_2O_2 system.[24]

Herein, a novel one-enzyme assisted exponential signal amplification strategy of target triggered K-junction structure digestion was proposed and used for the sensitive ECL detection of miRNA. As shown in Scheme 1, the K-junction structure, which was comprised of reporter DNA and substrate DNA was immobilized on an AuNPs-modified electrode *via* molecular self-assembly. The upper unpaired domains formed the recognition element and the reporter DNA was inhibited by the paired domain of the substrate DNA. Upon sensing the target, the 3′-terminus of reporter DNA and 5′-terminus of substrate DNA modified by phosphate paired with different domains of the target miRNA, respectively. After that, the substrate DNA was digested from the phosphate-modified 5′-terminus by lambda exonuclease until the paired domain was digested completely. Consequently, the undigested fragment of substrate DNA called the trigger DNA and the target miRNA were released and recycled, causing the linear and exponential digestion of the K-junction structure, respectively. Finally, the uninhibited reporter DNA was left on the electrode sufficiently to coordinate with the hemin. In addition, much more hemin/G-quadruplex chains were obtained to effectively catalyze the ECL reaction in the luminol/H_2O_2 system resulting in a significant enhancement of the ECL emission. Due to the high efficiency of the exponential signal amplification strategy, the detection process was significantly shortened to achieve the satisfactory sensitivity of miRNA in tumor cells.

Experimental

Reagents and material

Luminol (98%), hemin, gold chloride tetrahydrate ($HAuCl_4{\cdot}4H_2O$), tris(carboxy-ethyl) phosphine (TCEP) and 6-mercapto-1-hexanol (MCH) were obtained from Sigma-Aldrich Co. (St Louis, MO, USA). Hydrogen peroxide solution (30%) was purchased from Kelong Chemical Company (Chengdu, China). Lambda exonuclease (λ-exo) and 10 × λ-exo buffer were obtained from New England Biolabs, Inc. (Beverly, MA, USA). The other chemical reagents were of analytical grade. All of the DNA oligonucleotides (HPLC-purified) and the RNase inhibitor diethyl pyrocarbonate (DEPC) were obtained from Sangon, Inc. (Shanghai, China). The HPLC-purified miRNAs were synthetized by Takara Biotechnology (Dalian, China). Ethidium bromide (EB) was purchased from Beijing Dingguo Changsheng Biotechnology Co. Ltd (Beijing, China). The fetalbovineserum (FBS), penicillin and streptomycin were obtained from Hyclone (UT, USA). The two kinds of human cancer cell lines including human cervical cancer cell lines (HeLa) and human lung cancer cell lines (A549) were obtained from the Cell bank of type culture collection of the Chinese Academy of Science (Shanghai, China). The cells were grown in a humidified atmosphere with 5% CO_2 at 37 °C using Dulbecco's Modified Eagle's Medium supplemented with 10% FBS, 100 U mL^{-1} penicillin and 100 U mL^{-1} streptomycin. The buffer solutions used in this work were as follows: 1 × TE buffer (10 mM Tris-HCl, 1.0 mM ethylenediaminetetraacetic acid (EDTA), pH 8.0); 5 × TBE buffer (445 mM Tris base, 445 mM boric acid, 10 mM EDTA, pH 8.0); Tris-Mg buffer (10 mM $MgCl_2$, 10 mM NaCl, 20 mM Tris); phosphate-buffered solution (PBS) (0.1 M $Na_2HPO_4{\cdot}12H_2O$, 0.1 M KH_2PO_4, 0.1 M KCl, pH 7.4). A Hemin stock solution (0.25 mM) was prepared by dissolving hemin in PBS. A luminol stock solution (0.01 M) was prepared by dissolving luminol in NaOH solution (0.1 M) and stored at 4 °C in the dark until further use. All aqueous solutions were prepared with deionized water (specific resistance ≥18 MΩ cm). The sequence information of the nucleic acids used in this work is listed in Table 1.

Apparatus

ECL measurements were executed on a model MPI-A ECL analyzer (Xi'an Remex Electronic Science & Technology Co. Ltd, Xi'an, China) and the electrochemical measurements were conducted on a model CHI 660D electrochemistry workstation (Shanghai Chenhua Instruments, China). All experiments were carried out using a conventional three-electrode system.[25]

Table 1 The sequence information of the nucleic acids used in this work

Name	Sequences (5′ → 3′)
Reporter DNA	SH-$(CH_2)_6$-AAA AAC CAC TGG GTA GGG CGG GTT GGG AAC TGA TAA GCT A
Substrate DNA	PO_4-$(CH_2)_6$-TCA ACA TCA GTC CCA ACC CGC CCT ACC CAG TGA AAA GCT TAT CAG ACT GAT GTT GA
MiRNA-155	UUA AUG CUA AUC GUG AUA GGG GU
MiRNA-141	UAA CAC UGU CUG GUA AAG AUG G
MiRNA-199A	CCC AGU GUU CAG ACU ACC UGU UC
MiRNA-21	UAG CUU AUC AGA CUG AUG UUG A

Preparation of the non-denaturing polyacrylamide gel electrophoresis (PAGE)

To proceed the PAGE, six samples were prepared including: (a) 2 μM reporter DNA, (b) 2 μM substrate DNA, (c) 2 μM miRNA-21, (d) a mixture containing 2 μM reporter DNA and 2 μM substrate DNA, (e) a mixed solution containing 2 μM reporter DNA, 2 μM substrate DNA and 2 μM miRNA-21 and (f) a mixture, which was incubated under 37 °C for 1 h containing 2 μM reporter DNA, 2 μM substrate DNA, 2 μM miRNA-21 and 5 U lambda exonuclease. These samples were loaded into freshly made 16% polyacrylamide gel in 1 × TBE buffer at 120 V for 2 h. The gel was moved into darkroom to obtain electrophoresis image under UV light using a digital camera after being dyed with EB.

Fabrication of the biosensor

At first, GCE was carefully treated according to a previous report.[26] The obtained GCE was electrodeposited with gold nanoparticles (AuNPs) at a potential of −0.2 V for 30 s, followed by dropping the reporter DNA (10 μL, 1 μM) onto the surface and incubating for 16 h at room temperature. Then, MCH (10 μL, 1 mM) was incubated with the modified electrode for 30 min to block non-specific combination sites. After that, the substrate DNA modified by phosphate at the 5′-terminus (10 μL, 2 μM) was dropped onto the modified electrode. Before modification, the electrode was lightly washed several times with PBS.

Electrochemiluminescence measurements

A mixed solution (20 μL) containing the detection samples, λ-exo (5 U) and 1 × λ-exo buffer was dropped onto the prepared electrode and incubated for 1 h at 37 °C. Then, the electrode was washed with PBS to remove the unbound reagents and incubated with 10 μL of hemin stock solution (0.25 mM) for 45 min. Finally, the ECL response of the profiled biosensor was detected in PBS containing 50 μM luminol and 10 μM H_2O_2 at a scanning rate of 100 mV s^{-1} with a continuous potential scanning from 0.2 to 0.8 V.

Results and discussion

PAGE investigation for the formation and digestion of the K-junction structure

PAGE was executed to reveal the formation and digestion processes of the K-junction structure. In Fig. 1, the distinct single bands of the reporter DNA, substrate DNA and miRNA-21 were observed in lane a, b and c, respectively because of the different migration, which was mainly determined by the bases amount. Lane d, e and f show the PAGE results for the mixtures of reporter DNA/substrate DNA, reporter DNA/substrate DNA/miRNA-21 and reporter DNA/substrate DNA/miRNA-21/λ-exo, respectively. Lane d exhibits two distinct bands of unreacted reporter DNA (bottom band of lane d) and the hybridization of the reporter DNA and substrate DNA (top band of lane d), indicating that the reporter DNA/substrate

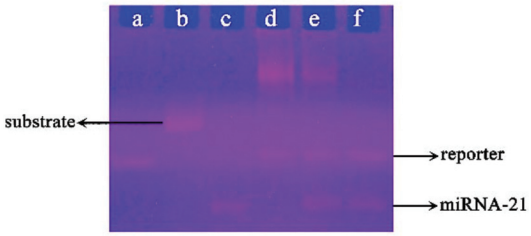

Fig. 1 PAGE characterization of the different samples. Lane a: 2 μM reporter DNA; lane b: 2 μM substrate DNA; lane c: 2 μM miRNA-21; lane d: 2 μM mixture of reporter DNA and substrate DNA; lane e: 2 μM mixture of reporter DNA, substrate DNA and miRNA-21; lane f: a mixed solution containing 2 μM reporter DNA, 2 μM substrate DNA, 2 μM miRNA-21 and 5 U λ-exo (incubated at 37 °C for 1 h). All of the samples were heated to 95 °C and kept for 5 min to gradually cool to room temperature naturally.

DNA complex was formed. Lane e displays three recognizable bands suggesting that there was unreacted miRNA-21 present. Due to the bases amount of miRNA was only 22, it was undistinguishable between the top band of lane d and e. As expected, lane f exhibited two clear bands with nearly identical mobility to the reporter DNA and miRNA-21, respectively, which was due to the cleavage of λ-exo for the substrate DNA. The PAGE results indicated the successful formation of the K-junction structure and the digestion of the K-junction structure in the presence of miRNA-21.

Electrochemical characterization of the proposed biosensor

To confirm the fabrication of the biosensor, cyclic voltammetry (CV) and electrochemical impedance spectroscopy (EIS) experiments were carried out in a 5.0 mM $[Fe(CN)_6]^{3-/4-}$ solution. As exhibited in Fig. 2A, a pair of reversible redox peaks were observed when the measurement was executed with the bare GCE (curve a). After electrodeposition of the AuNPs, the peak current was significantly increased (curve b) due to the good conductivity of the AuNPs. Then, the peak current was decreased (curve c) after the reporter DNA was incubated, since the DNA obstructs the electron transfer. With the non-specific bond sites blocked by MCH, the peak current was further decreased (curve d). Following the immobilization of the sub-

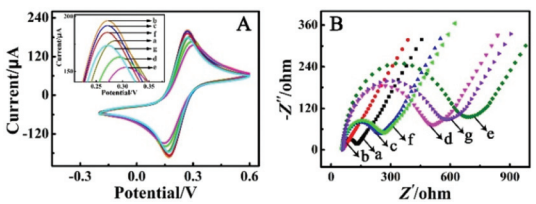

Fig. 2 The CV (A) and EIS (B) experiments of the proposed biosensor: (a) bare GCE, (b) AuNPs/GCE, (c) reporter DNA/AuNPs/GCE, (d) MCH/reporter DNA/AuNPs/GCE, (e) substrate DNA/MCH/reporter DNA/AuNPs/GCE, (f) miRNA-21 and λ-exo/substrate DNA/MCH/reporter DNA/AuNPs/GCE and (g) hemin/miRNA-21 and λ-exo/substrate DNA/MCH/reporter DNA/AuNPs/GCE. The modified electrodes were tested in 5.0 mM $[Fe(CN)_6]^{3-/4-}$.

strate DNA onto the electrode, the peak current was persistently decreased (curve e) because the hybridization DNA chains hindered the electron transfer. Subsequently, after incubation with miRNA-21 and λ-exo, the peak current was increased (curve f), indicating the successful cleavage of the substrate DNA. As expected, the current was decreased sequentially after incubation with hemin (curve g), indicating that the electron transfer was impeded by the hemin/G-quadruplex because of the repulsive effect among each component.

EIS was also used to characterize the electrode surface modification. Fig. 2B shows the bare GCE (curve a) has a much larger semicircle diameter than the AuNPs coated GCE (curve b). When the negatively charged reporter DNA (curve c), non-conductive MCH (curve d) and negatively charged substrate DNA (curve e) were incubated sequentially, the semicircle diameter was increased consecutively. However, the semicircle diameter was decreased after incubation with the mixture of miRNA-21 and λ-exo (curve f). Finally, the semicircle diameter was increased when hemin was assembled (curve g). These results were coincident with the results of the CV, suggesting that the biosensor was successfully fabricated.

ECL characterization of the biosensor fabrication

The ECL characterization was further used to investigate the fabrication process of the biosensor in PBS containing a luminol stock solution (50 μM) and H_2O_2 (10 μM). As displayed in Fig. 3, the bare GCE was detected at first (curve a). When the electrode was coated with the AuNPs, the ECL intensity was significantly increased, which was attributed to the acceleration of electron transfer by the AuNPs (curve b). After immobilization of the reporter DNA (curve c), the ECL intensity was slightly decreased, due to the electron-repulsion between $[Fe(CN)_6]^{3-/4-}$ from the modified-electrode surface and the negatively charged phosphate backbones of the reporter DNA. Following the incubation with MCH (curve d), the ECL intensity was further decreased because MCH significantly hindered the electron transfer. In a similar way, the ECL intensity was decreased upon incubation with the substrate DNA (curve e). When miRNA-21 and λ-exo were introduced on the prepared electrode, the ECL intensity was enhanced (curve f) due to the fact that the substrate DNA was cleaved and the uninhibited reporter DNA was left on the electrode. When incubated with hemin, the ECL signal was remarkably amplified (curve g). This was attributed to the catalysis effect of the hemin/G-quadruplex for the decomposition of H_2O_2.

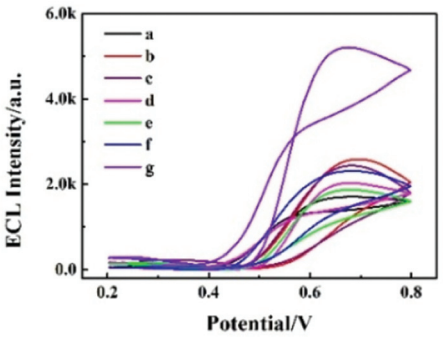

Fig. 3 The ECL performance of the assembled biosensor step by step: (a) bare GCE, (b) AuNPs/GCE, (c) reporter DNA/AuNPs/GCE, (d) MCH/reporter DNA/AuNPs/GCE, (e) substrate DNA/MCH/reporter DNA/AuNPs/GCE, (f) miRNA-21 and λ-exo/substrate DNA/MCH/reporter DNA/AuNPs/GCE and (g) hemin/miRNA-21 and λ-exo/substrate DNA/MCH/reporter DNA/AuNPs/GCE. The stepwise detection was accomplished in PBS containing 50 μM luminol solution and 10 μM H_2O_2 by scanning the potential from 0.2 to 0.8 V.

Optimization of the experimental conditions used for the ECL biosensor

The incubation time of miRNA-21, λ-exo and hemin were optimized to obtain the optimal performance of the biosensor. Fig. 4A reveals the effect of the incubation time of miRNA-21 and λ-exo. With an increase in the incubation time of miRNA-21 and λ-exo, the ECL response was enhanced gradually and the maximum ECL response was obtained at 60 min. Thus, the ECL measurements were carried out incubating the miRNA-21 and λ-exo for 60 min. Fig. 4B displays the effect of the incubation time with hemin. The ECL signal was enhanced as the time increased and then reached a plateau after 45 min. As a result, the incubation time with hemin was 45 min in the following experiments.

MiRNA-21 detection using the proposed ECL biosensor

In order to estimate the properties of this biosensor, the ECL signals were measured using the optimized conditions with different concentrations of miRNA-21. The relevancy between the ECL response and miRNA concentration is displayed in Fig. 5. Obviously, the ECL intensity was gradually increased upon increasing the concentration of miRNA-21. The inset displays the linear relationship of the ECL intensity and the logarithm of miRNA-21 concentration from 1.0×10^{-15} M to 1.0×10^{-9} M with a detection limit of 0.033 fM. In addition, the linear equation was $I = 8574.82 + 327.09 \log(c/\mathrm{M})$ (where I represents the ECL intensity and c is the concentration of miRNA-21) with a correlation coefficient of 0.9959.

The selectivity and stability of the biosensor

Proceeding from the application of the biosensor, the selectivity is a significant property. Contrast experiments were per-

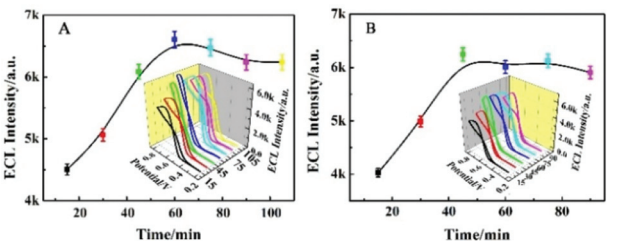

Fig. 4 (A) Optimization of the incubation time of miRNA-21 and λ-exo. (B) Optimization of the incubation time of hemin. All the ECL intensities were detected in PBS containing 50 μM luminol solution and 10 μM H_2O_2 solution by scanning the potential from 0.2 to 0.8 V.

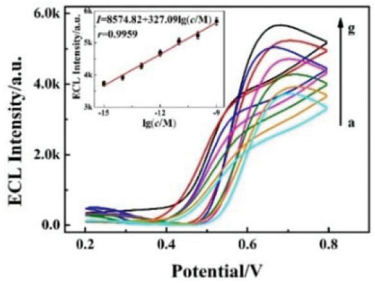

Fig. 5 ECL profiles of the biosensor with different concentrations of miRNA-21: (a) 1.0×10^{-15} M, (b) 1.0×10^{-14} M, (c) 1.0×10^{-13} M, (d) 1.0×10^{-12} M, (e) 1.0×10^{-11} M, (f) 1.0×10^{-10} M and (g) 1.0×10^{-9} M. The inset shows the calibration curve used for miRNA-21 detection. All the ECL measurements were completed in PBS containing 50 μM luminol solution and 10 μM H_2O_2 solution with the scanning potential from 0.2 to 0.8 V.

formed using different miRNAs containing miRNA-199A, miRNA-141 and miRNA-155 to replace miRNA-21 with identical concentration (1.0×10^{-10} M), respectively. As shown in Fig. 6A, miRNA-21 and a mixed solution containing an approximate concentration (1.0×10^{-10} M) of miRNA-199A, miRNA-141, miRNA-155 and miRNA-21 induced remarkable ECL responses, whereas the ECL responses were negligible in the presence of the non-target miRNAs. Moreover, the ECL signals of the non-target miRNAs were barely changed in comparison with the blank test. There was an inconspicuous difference between the single miRNA-21 and the mixed sample, which means the non-target miRNAs had little influence on the ECL response of the target miRNA. These results indicated that the proposed ECL biosensor presented a high specificity and selectivity for miRNA-21 detection.

The stability of the ECL biosensor is another important factor to estimate its performance. In Fig. 6B, the ECL intensity was consistent when subjected to continuous cyclic potential scans for 11 cycles with a relative standard deviation (R.S.D.) of 1.05%. The experimental results indicated that the ECL biosensor had good stability.

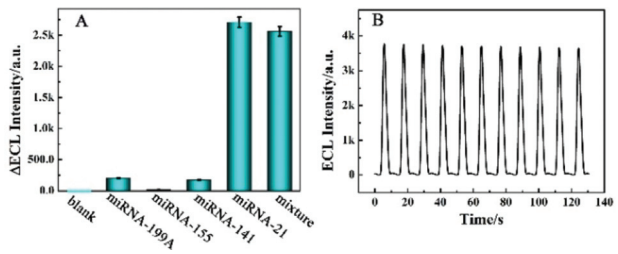

Fig. 6 (A) The ECL signals with the different samples: blank; miRNA-199A (1.0×10^{-10} M); miRNA-155 (1.0×10^{-10} M); miRNA-141 (1.0×10^{-10} M); miRNA-21 (1.0×10^{-10} M) and a mixed solution of all the miRNAs. (B) The stability of proposed biosensor after consecutive cyclic potential scans for 11 cycles when the concentration of miRNA-21 was 1.0×10^{-15} M. All of the ECL measurements were completed in PBS containing 50 μM luminol solution and 10 μM H_2O_2 solution by scanning the potential from 0.2 to 0.8 V.

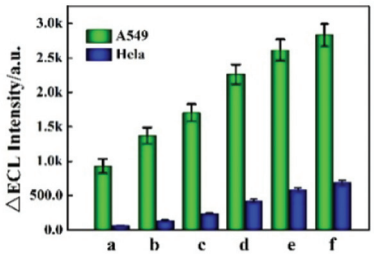

Fig. 7 MiRNA-21 detection in different tumor cell lines: (a) 1.0×10^1 cells, (b) 1.0×10^2 cells, (c) 1.0×10^3 cells, (d) 1.0×10^4 cells, (e) 1.0×10^5 cells and (f) 1.0×10^6 cells of A549 cell lines and HeLa cell lines, respectively.

Application of the ECL biosensor in tumor cells

Based on the previous literature reports, the practical applicability of our method for miRNA detection was investigated in real biological samples upon increasing the cell number of HeLa cell lines and human lung adenocarcinoma cell lines (A549 cell lines). According to the assay results, miRNA-21 was in distinguishable expression levels in the different cell lines (Fig. 7). The ECL signal was slightly increased upon increasing the amount of HeLa cell lines, while an obviously increased ECL signal was achieved in the A549 cell lines from 1.0×10^1 cells to 1.0×10^6 cells. This means that the miRNA-21 was overexpressed in the A549 cell lines when compared with the HeLa cell line, which was in good agreement with the present research results.[3,27] These results indicate that the ECL biosensor was able to monitor the miRNA biomarkers in biological samples.

Conclusions

In summary, a sensitive K-junction structure mediated exponential signal amplification strategy was proposed and applied in an ECL biosensor for miRNA detection. Upon sensing the target miRNA, the substrate DNA in the K-junction structure is exponentially digested by λ-exo. As a result, a mass of uninhibited reporter DNAs are activated on the electrode to capture hemin to produce significant amounts of the hemin/G-quadruplex, which significantly amplified the ECL signal in the luminol-H_2O_2 system. Based on the high-efficiency exponential signal amplification strategy and the ECL enhancement of the hemin/G-quadruplex, the proposed ECL biosensor has achieved excellent performance in miRNA-21 detection, which meets the requirements of its application in tumor cells. The results indicate that this strategy has enormous potential for further application in monitoring different nucleic acids.

Acknowledgements

This work was financially supported by the National Natural Science Foundation (NNSF) of China (21575116, 51473136 and 21675129) and the Fundamental Research Funds for the Central Universities (XDJK2016E056), China.

References

1 P. B. Zhang, J. Y. Zhang, C. L. Wang, C. H. Liu, H. Wang and Z. P. Li, *Anal. Chem.*, 2014, **86**, 1076–1082.
2 H. Tian, Y. Y. Sun, C. H. Liu, X. R. Duan, W. Tang and Z. P. Li, *Anal. Chem.*, 2016, **88**, 11384–11389.
3 Y. Liao, R. Huang, Z. K. Ma, Y. X. Wu, X. M. Zhou and D. Xing, *Anal. Chem.*, 2014, **86**, 4596–4604.
4 E. M. Harcourt and E. T. Kool, *Nucleic Acids Res.*, 2012, **40**, e65.
5 T. Hou, W. Li, X. J. Liu and F. Li, *Anal. Chem.*, 2015, **87**, 11368–11374.
6 S. S. Lu, T. Hu, S. Wang, J. Sun and X. R. Yang, *ACS Appl. Mater. Interfaces*, 2017, **9**, 167–175.
7 Y. Zhu, H. J. Wang, L. Wang, J. Zhu and W. Jiang, *ACS Appl. Mater. Interfaces*, 2016, **8**, 2573–2581.
8 F. Z. Xu, H. Shi, X. X. He, K. M. Wang, D. G. He, Q. P. Guo, Z. H. Qing, L. A. Yan, X. S. Ye, D. Li and J. L. Tang, *Anal. Chem.*, 2014, **86**, 6976–6982.
9 J. P. Zhang, C. Li, X. Zhi, G. A. Ramón, Y. L. Liu, C. L. Zhang, F. Pan and D. X. Cui, *Anal. Chem.*, 2016, **88**, 1294–1302.
10 Y. F. Lv, L. Cui, R. Z. Peng, Z. L. Zhao, L. P. Qiu, H. P. Chen, C. Jin, X. B. Zhang and W. H. Tan, *Anal. Chem.*, 2015, **87**, 11714–11720.
11 Z. Z. Zhang and C. Y. Zhang, *Anal. Chem.*, 2012, **84**, 1623–1629.
12 Y. Gao and B. X. Li, *Anal. Chem.*, 2014, **86**, 8881–8887.
13 Y. Gao, X. Y. Liu, W. J. Qi, W. Y. Gao, Y. H. Li and G. B. Xu, *Analyst*, 2015, **140**, 3996–4000.
14 F. Wang, J. Lin, T. B. Zhao, D. D. Hu, T. Wu and Y. Liu, *J. Am. Chem. Soc.*, 2016, **138**, 7718–7724.
15 H. B. Habtamu, M. Sentic, M. Silvestrini, L. De Leo, T. Not, S. Arbault, D. Manojlovic, N. Sojic and P. Ugo, *Anal. Chem.*, 2015, **87**, 12080–12087.
16 H. J. Wang, L. J. Bai, Y. Q. Chai and R. Yuan, *Small*, 2014, **10**, 1857–1865.
17 L. L. Li, Y. Chen and J. J. Zhu, *Anal. Chem.*, 2017, **89**, 358–371.
18 G. Z. Ma, J. Y. Zhou, C. X. Tian, D. C. Jiang, D. J. Fang and H. Y. Chen, *Anal. Chem.*, 2013, **85**, 3912–3917.
19 B. Haghighi, A. Tavakoli and S. Bozorgzadeh, *Electrochim. Acta*, 2015, **154**, 259–265.
20 Z. Q. Gao, M. D. Xu, M. H. Lu, G. N. Chen and D. P. Tang, *Biosens. Bioelectron.*, 2015, **70**, 194–201.
21 J. Zhang, J. P. Wang, L. Yang, B. H. Liu, G. J. Guan, C. L. Jiang and Z. P. Zhang, *Chem. Commun.*, 2014, **50**, 15870–15873.
22 J. X. Wang, Y. Zhuo, Y. Zhou, H. J. Wang, R. Yuan and Y. Q. Chai, *ACS Appl. Mater. Interfaces*, 2016, **8**, 12968–12975.
23 Y. Zhuo, M. N. Ma, Y. Q. Chai, M. Zhao and R. Yuan, *Anal. Chim. Acta*, 2014, **809**, 47–53.
24 P. Zhang, X. Y. Wu, R. Yuan and Y. Q. Chai, *Anal. Chem.*, 2015, **87**, 3202–3207.
25 B. Yang, J. P. Li, L. M. Zhang and G. B. Xu, *Analyst*, 2016, **141**, 5822–5828.
26 Y. Zhang, X. H. Pang, D. Wu, H. M. Ma, Z. Q. Yan, J. T. Zhang, B. Du and Q. Wei, *Analyst*, 2016, **141**, 337–345.
27 B. C. Yin, Y. Q. Liu and B. C. Ye, *J. Am. Chem. Soc.*, 2012, **134**, 5064–5067.

